Web-based Visualisation for Look-Ahead Ground Imaging in Tunnel Boring Machines

Lijun Wei[1,*], Muhammad Khan[1], Owais Mehmood[2], Qingxu Dou, Carl Bateman, Derek R. Magee, Anthony G. Cohn

School of Computing, University of Leeds, Leeds, United Kingdom

Abstract

Tunnel Boring Machines (TBMs) are large multi-million pound machines used to excavate underground tunnels. In order to make best use of the high-speed performance of a TBM and guarantee the safety of excavation, it is important to know the local geology, structures and ground properties ahead of the TBM cutter head, especially in complex geological conditions (e.g. karst caves). By working with experienced geophysical experts, tunnelling engineers/consultants and TBM manufacturers, we propose a novel web-based visualisation platform to help TBM operators efficiently manage, process and visualise the TBM parameters, the geology map created by geo-experts based on boreholes, and especially the imaging data captured by an on-board ground imaging system for "seeing through" the ground beyond the excavation surface. Informative visualisation interfaces were designed to facilitate interpretation of the imaging data and adding annotation by users; algorithms were developed for automatic detection of features and probable events by fusion of radar and seismic imaging data; and a back-end database was designed to store all such relevant information for supporting more advanced interpretation in the future. The web-based architecture not only allows the visualisation platform to be directly linked to on-board sensors (e.g. ground penetrating radars, seismic sensors), but also allows users away from the job site to access the captured data using a standard web browser, enabling a collaborative interpretation process. The data processing, management and visualisation platform presented in this paper is flexible with respect to different imaging sensors and modalities, so it is highly adaptable for any other ground imaging systems for tunnel geology inspection, underground utility surveys, etc.

Keywords: Ground prediction system, Visualisation, GPR, Seismic sensors

1. Introduction

Tunnel Boring Machines (TBMs) are large multi-million pound machines used to excavate underground tunnels. Compared with traditional drilling-and-blasting techniques, TBMs have a much higher rate of excavation; for example, they can progress at the rate of 70 metres a day (typically around 30 to 40 metres a day). They can also reduce rock damage, labour costs and generate smoother tunnel internal surfaces [1]. However, TBMs generally have low adaptability and flexibility to local geological variations [2]. For example, sudden geological changes might necessitate a change of drag bits on the TBM face; man-made artefacts such as deep foundations of buildings may obstruct the excavation; and groundwater in adverse geological bodies (e.g. karst caves, coal mine collapse column) might flood a tunnel [3]. These local geological variations can significantly influence the TBM advance rate, rock fragmentation efficiency, cutter head wearing and deform or damage the TBM, resulting in delay of construction progress, or even cause loss of property and life. In order to make best use of a TBM and its high-speed performance and guarantee the safety of excavation, it is important to have the information of local geology structure ahead of the TBM cutter head.

Surface and borehole geological surveys are usually performed at sampling locations along the route of a tunnel, but the interpolated geological maps are not sufficiently accurate for predicting the local geological variations. In order to evaluate the short-range ground conditions ahead of the tunnel face, Leu et al. [4] used a neural network and Guan et al. [5] used a Markov random process to predict the ground conditions based on excavated materials, whilst Yamamoto et al. [6] used geostatistical techniques to analyse the TBM driving data and the drill logging data from pilot boring at the same time. The local variations can also be detected by ground imaging/prediction systems [1] equipped with non-destructive geophysical sensors [7, 8, 9] by measuring the differences in the propagation velocity of mechanical waves in various media using methods like tunnel seismic prediction (TSP) [10, 11, 12], analysing the differences in the electrical permittivity of the media based on the propagation of electromagnetic waves using methods like transient electromagnetic technique [7] and ground penetrat-

*Corresponding author. Tel: +44 (0)113 343 5430. Postal address: School of Computing, University of Leeds, LS2 9JT, Leeds, United Kingdom

Email addresses: l.j.wei@leeds.ac.uk (Lijun Wei), mskhan@trunarrative.com (Muhammad Khan), owais.mehmood@york.ac.uk (Owais Mehmood), douqx2005@hotmail.com (Qingxu Dou), carlbateman@hotmail.com (Carl Bateman), d.r.magee@leeds.ac.uk (Derek R. Magee), a.g.cohn@leeds.ac.uk (Anthony G. Cohn)

[1]The first two authors are the lead authors of the paper.

[2]Owais Mehmood is now at the University of York; his contribution to this paper was performed whilst employed at the University of Leeds.

ing radar (GPR) [13, 14, 15, 16][3], or analysing the shape of the electrical or magnetic field which is generally obtained by measuring the electrical resistivity [18]. To reduce the cost and improve the operability of ground imaging systems, data acquisition should not interrupt tunnelling operations, which means that these systems should operate in stopped time of the TBM operation with fast, frequent and effective acquisition procedure, be fully integrated on-board the TBM with an open and flexible system architecture and expandable for adding other subsystems [1]. However, most of the current methods require dedicated periods of time for data capture and analysis during which other tunnel construction activities must be stopped.

In addition to the ground imaging system itself, imaging data transmission, storage, analysis and especially visualisation are also crucial for effective data interpretation, a complex process requiring specific skills and expertise. Informative visualisation can maximise the value of the captured data and facilitate data interpretation and decision-making by TBM operators/geo-experts. Several visualisation systems have been developed to help geophysical data interpretation for various purposes [19, 20, 21]. For example, [19] developed a visualisation system for interpreting geophysical data from archaeological sites, [20] presented a system for processing and visualising ground penetrating radar data for measuring pavement thickness, and [21] proposed a system for representing the buried utility data and the movement of excavation equipment in a 3D visualisation environment. Systems have also been developed for visualising the tunnel environment [22, 23, 24, 25, 26]. For example, [22] developed a system for visualising the construction data of shield tunnels such as tunnel geometries and attributes, [23] used virtual reality technology to visualise the tunnel construction environment, [24] proposed a tunnel modelling and visualisation system based on real-time TBM tracking and positioning data, [25] proposed a tunnel information system for managing and using the geo-engineering data in urban tunnel projects, and a system was developed by [26] for safety risk early warning in urban metro constructions based on fusion of multisource information (monitoring measurements, calculated predictions, and visual inspections), but none of these work managed or visualised the geophysical data in tunnels. To the best of the authors' knowledge, there is no work in the literature focusing on addressing the data management and visualisation problem for tunnel ground prediction/imaging systems.

1.1. Our Contribution

In this work, we present a novel web-based visualisation platform that can be connected to a Look-Ahead Ground Imaging System on Tunnel Boring Machines for detecting and visualising the local geological anomalies ahead of the TBM cutter head. The platform was developed by working closely with experienced geophysical experts, tunnelling engineers, consultants and TBM manufacturers and following an iterative design/testing process to choose the most appropriate solutions. It has the functions of data transmission/storage, 2D/3D visualisation and human-machine interactive data interpretation with the support of informative and user-friendly interfaces. Dedicated GPR and seismic sensors were designed by our project partners [27, 28, 29, 30] within the EU funded NeTTUN[4] project and included in the connected *Look-Ahead Ground Imaging System* [9] in order that these sensors can complement each other in different challenging situations (e.g. a GPR may not work properly in damp environment) based on both dielectric and elastic properties of the ground. Both imaging data and relevant contextual data, such as the initial geological survey data along a tunnel route (in the form of initial geology maps or simplified geology) and TBM operational data (e.g. ground pressure, cutter head torque) are stored and visualised to help data analysis. It should be noted that the focus of this paper is not on the sensor design but the fusion and visualisation of the sensor data once obtained.

Our contribution in this work is threefold. Firstly, since ground imaging data interpretation is a complex process requiring specific skills and expertise, the web-based design allows both on-site and remote data accessing by engineers in and outside the tunnel, establishing real-time interaction and collaboration between them for situation analysis. By fusion and visualisation of the ahead-looking imaging data from different perspectives and overlaying the related geological context and TBM parameters, users can gain a better understanding of what could be uncovered by subsequent excavation. Secondly, the back-end database stores the imaging data and the contextual information (e.g. TBM parameters, geological maps, experts' annotation before and after excavation and their explanation) about the adverse geological events in different tunnelling projects and can be used as an evidence base to enhance users' (e.g. junior engineer) understanding of imaging data interpretation. As more data from real tunnelling projects is fed in, machine learning techniques can be developed in the future to further help the interpretation of hazardous events. If the GPS coordinates of tunnel segments are given, the proposed platform can also serve as a geographic information system (GIS) to spatially manage the imaging data from different tunnelling projects and visualise the geological background in a broader context to help data analysis [31, 32]. Thirdly, the visualisation platform presented in this paper is quite flexible to the selected models (e.g. sensor frequencies) and configurations (e.g. size/shape of the scanning pattern) of the imaging sensors, so the platform is also applicable to other ground imaging systems used on tunnel boring machines or surface geophysical survey equipment [33]. We have not found a similarly flexible and widely scoped web-based visualisation system for sensor data described in the literature.

The rest of the paper is organised as follows: section 2 introduces the architecture of the proposed platform; section 3 presents the data acquisition procedure, the communication protocol and database design; section 4 presents the visualisation and image analysis components, followed by discussion in

[3]A review of current practices and the potential of using ultra-wide band (UWB) radar for cost-effective, non-destructive detection in underground construction is given in [17].

[4]NeTTUN: `https://web.archive.org/web/20170601061958/http://nettun.org/`. Accessed: 2019-04-25.

section 5 and conclusions in section 6.

2. System Architecture of The Proposed Visualisation Platform

The architecture and general work flow of the platform is shown in Figure 1. At first, GPR and seismic data is captured, pre-processed and stored on a file system. When the pre-processed data at a certain chainage[5] is ready (notified by a data ready protocol), the image analysis component is initiated for detection and tracking of anomalous features and events across multiple sensor images; the corresponding databases of sensor data and features/events are also updated. Then, for a specific tunnel ring[6] selected by the user, the visualisation platform accesses the database and visualises the images and relevant contextual data. It also allows human operators to access and manually update the nature of the detected events and to add additional annotations through the user interface. The users' interpretations are stored as attributes of the tagged features.

A prototype has been developed to demonstrate the functionality of the proposed web-based information platform and to provide guidance for further development and improvement. The prototype is implemented as a web application with both server and client sides: the server side is implemented using *C++* based on *POCO* library[7] and consists of a centralised data repository, a data interpretation service, and a communication protocol with the data acquisition system; the browser-based client side is developed with *html/javascript/CSS/Ajax* and *WebGL* that runs within a web browser to interact with the server. The prototype has been successfully tested on a variety of browsers including Internet Explorer, Firefox and Chrome. No special requirements are needed for the hardware and software on the client's computer. More details of each component will be given in the following sections.

3. Data Acquisition and Data Management

This section briefly introduces the geophysical sensors used for data acquisition, the data ready communication protocol between the data acquisition system and the data analysis/visualisation component, and the back-end database designed for data management.

3.1. Data Acquisition

The ground imaging system was designed for soft ground tunnelling operations and consists of multiple sets of GPR antennae tuned to different frequencies as well as a shear-wave seismic imaging system. The operation concept of the system is to "image" the front with GPR and seismic sensors installed on the TBM cutter head and oriented forward while the TBM is not excavating. This operation is repeated each time a ring is being erected, i.e. every few metres along the tunnel axis. The architecture of the system is designed to be open and flexible, offering built-in scalability with respect to the TBM diameter and type, and expandability through the potential addition of other complementary subsystems [9].

To collect data for all sensing modalities, instead of capturing several transects of data on a measurement grid, the data is alternatively captured by scanning when rotating the cutter head (Figure 2) [9]. Dedicated seismic sources and receivers were placed along a diameter of the cutter head (Figure 2(b)) to generate and record seismic shear waves on three angular planes for further inversion analysis [30, 29]. In order to achieve the best coverage and imaging resolution of the ground in front of the TBM cutter head by GPR, three sets[8] of complementary GPR antennae (each pair with a transmitter and a receiver) were designed: a low frequency GPR (with a bandwidth of 100-7600 MHz) to provide a large inspection range and two high frequency GPR sensors (with bandwidth between 450-1450 MHz) to detect small-sized targets like rock fractures which might only be a few centimetres in length [27, 28]. In order to protect the GPR instrument during the excavation process, a 3 cm thick epoxy resin plate was placed between the dipoles and the ground to protect the GPR antenna from blows and external pressure when mounted on the TBM [27]. The interference between the GPRs and the TBM was also considered when designing the sensors [28]. During the acquisition, the three GPR sensors (with different frequencies) are placed on three different radii sequentially and the TBM is rotated in an anti-clockwise direction at a constant rate (Figure 2(a)). In so doing, nine GPR images can be generated at each TBM location [15, 16, 28]. The data acquisition process is controlled by bespoke data acquisition software and hardware designed by the NetTUN partner Geo2X (Switzerland) and the imaging process is repeated whilst each tunnel segment ring is erected along the tunnel axis. Examples of data acquired by the GPR and seismic sensors (after pre-processing) are shown in Figure 8 and 13.

3.2. Data Ready Communication Protocol (DRCP)

Once imaging data is acquired and ready, a Data Ready Communication Protocol (DRCP) is used to notify the data processing/visualisation platform. DRCP is based on a client-server architecture for data transmission using TCP stream sockets[9] with communication messages in *XML* format. Here the client is the data provider (the data acquisition software, e.g. GPR) which initiates the protocol by sending a data signal to the server using an *XML* file. This particular *XML* message is in a human-readable format with possibilities for future extension. It contains all the necessary information about the captured data such as the number of files, type of files (e.g. GPR images) and location of those files. With this message, the visualisation server

[5]Chainage is the distance measured in metres along the centre line of a tunnel route from a defined start point.

[6]We assume that concrete lining ring are inserted every few metres along the tunnel length.

[7]POCO: a C++ based library for network-centric and portable applications development. It can be used for cross-platform and real-time applications.

[8]We chose three sets for the initial prototype, More, or fewer, sets could be easily accommodated in our visualisation platform.

[9]Transmission Control Protocol (TCP) is a reliable socket protocol which treats communication as a continuous stream of characters.

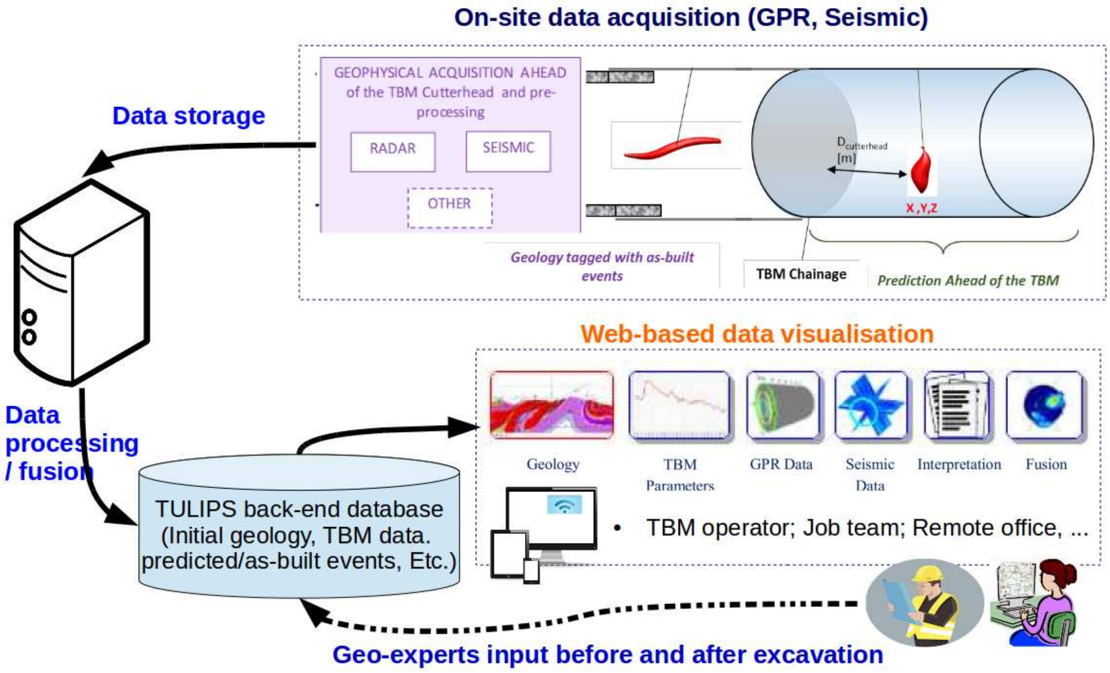

Figure 1: Work flow of the web-based information platform for management, visualisation and interpretation of tunnel ground imaging/contextual data.

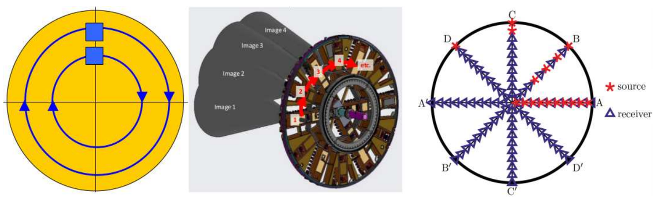

(a) GPR circular scanning options [9] (b) Seismic sensors [30].

Figure 2: Circular scanning configuration of the ground imaging system. (a) GPR sensors; (b) Cutter head of the TBM showing source-receiver acquisition geometries along different diameters [30]

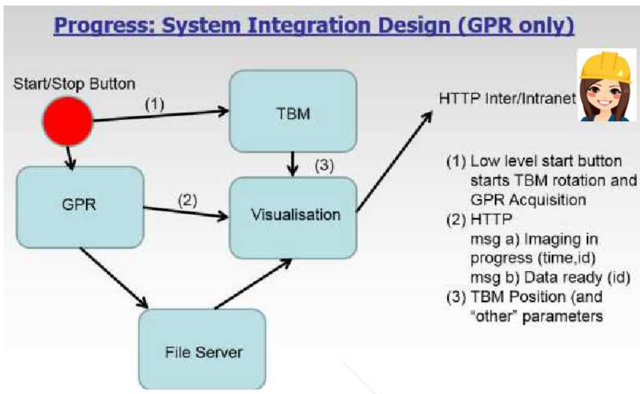

Figure 3: System architecture for communication between the data capturing system, TBM and the visualisation platform (GPR is demonstrated as an example).

initiates the process of data downloading and updating the corresponding database. Communication errors, which may affect the data ready exchange, are handled using the standard Transmission Control Protocol in the POCO C++ library. The system architecture for the communication protocol is shown in Figure 3.

3.3. Data Management and Database Design

In this platform, a back-end database was designed and implemented to store and manage the imaging information (e.g. the captured imaging data, the anomalous geological features/events predicted by a feature detection algorithm or annotated by human experts), the surveyed geology data (in the form of initial geology maps) and the TBM parameters from different tunnelling projects. The stored data from historical projects could be used for assisting decision making in future projects.

Database of Captured Imaging Data. This database stores the system parameters and attributes of each captured GPR and seismic image. It includes three tables: 1) table ***Project_constants*** stores the parameters/constants used by the ground imaging system in a project, such as the starting angle of the data acquisition (e.g. 0.000 degree with respect to a fixed direction) and the scanning direction (e.g. CCW: counter-clockwise); 2) table ***gpr_data*** stores the information of each captured GPR image; 3) and table ***seismic_data*** stores the information of each seismic image obtained by inverse modelling. The three tables are linked by their *Project ID*. Structures of the three tables is shown in Appendix Figure A.19. Once the meta-data file of a captured image is received by the server, the corresponding image database is updated.

Database of Detected Features and Events. An event is a local change in geology (e.g. fault, karst) or man-made artefacts (building foundation, pipe). Features are the local changes in sensor data that could indicate the presence of an event, which could correspond to a single or multiple features in different sensor data (i.e. multiple features contribute to the same event). A feature can be detected automatically from the sensor data or manually annotated by human experts. This database was designed to store the attributes of detected/annotated features, events and the correspondences between them. It includes four tables: 1) In the ***Feature*** table, a feature can be uniquely identified by its *feature ID* and *project ID*. This table also stores the local 3D location of a feature with respect to the TBM front plane and centre, its feature chainage[10] in the tunnel, its latitude and longitude, whether it is an artefact and whether it is an auto detection or manually annotated. For the purpose of visualisation, the geometry shape (e.g. ellipse, box, curve) used to represent the features is also stored together with the corresponding shape parameters. For example, the information of curves is stored in a separate table *Curve*, in which each curve is represented by a list of curve/boundary points (multiple points in $\{x, y, z\}$ format). 2) An ***Event_type*** table is designed to store various types of events that might be encountered, i.e. one of {*Brutal Change, Fault, Inclusion, Karst, Piles, Foundation, Pipes, Slow Transition, Water Inflow, Unknown*}. 3) The information of each detected event is stored in the ***Event*** table and is assigned a specified *event type* that is linked to the *Event Type* table. 4) As an event can correspond to one or multiple features, an ***Event_Feature*** table is designed to capture these correspondences. Note that an event can occur only once but multiple features (non-repeated) can relate to the same event. Relationship diagram of the feature and event database is shown in Appendix Figure A.20.

Database of Simplified Tunnel Geology. In addition to the imaging database, a tunnel geology database is designed to describe the geology data along the tunnel route to help human operators understand the broad context and facilitate data interpretation. As a tunnel route can be divided into several segments and the ground in each segment can be composed of various materials such as rock, clay and minerals, three tables are designed to capture this information: 1) the ***Tunnel_Segments*** table stores the locations of segments[11] in a tunnel including segment chainage and segment descriptions; 2) the ***Material_Type*** table stores the various material types a tunnel could be composed of; 3) and the ***Segment_Geology*** table links the *Tunnel_Segments* and *Material_Type* tables to store the specific geology information around each tunnel segments. The relationship diagram of the tunnel geology database is shown in Appendix Figure 21(a).

Database of TBM Parameters. The data of TBM parameters is acquired by the TBM Programmable Logic Controller (PLC) from various sources, including external sensors and internal TBM operating systems. As real-time TBM parameters are largely affected by and may also reflect the front ground conditions [6], tables are designed to store the information collected by the sensors on TBM, such as ground pressure, cutter head torque, cutter head rotation speed, and thrust force. TBM parameters are associated with corresponding chainages and stored in three tables: 1) the ***TBM Parameters*** table stores the various types of TBM parameters; 2) the ***TBM_Segment*** table stores the information of each segment with its start chainage and end chainage; 3) and the ***TBM_Data*** table stores the values of different TBM parameters in different segments. The relationship diagram of TBM parameter database is shown in Appendix Figure 21(b).

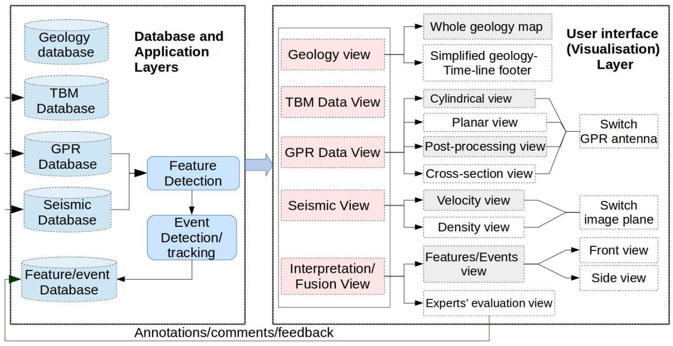

Figure 4: The components and functionality of the visualisation platform.

4. 2D/3D Visualisation and Events Detection Component

As mentioned in Section 3, once the captured imaging data is downloaded on the visualisation server, it can be visualised in the user interface and used for interpretation of probable events. The related database is also updated. In order to perform a full analysis of the front condition, several visualisation interfaces were developed, including geology view, TBM data view, GPR data view, seismic view and interpretation view (Figure 4). The visualisation platform allows users to change the data displayed, select the time point, and switch between different visualisation methods. It also allows experts to add annotation for probable events before and after the tunnel excavation.

Basic layout of the user interface is shown in Figure 5. The design principle behind this layout is to tackle the problem that one screen size is typically not large enough to display all the imaging and contextual data for interpretation simultaneously. *Navigation buttons* are provided at the top of the interface to allow users switch between different data (geology, TBM parameters, GPR data, seismic data, human/machine interpretation results). The *visualisation window* in the middle is the main window for visualising different data. Meanwhile, in order to switch between different tunnel locations where imaging data is captured, a time-line with *pins* is designed near the bottom of the user interface. The pins represent the tunnel rings/chainage and users can click on individual pins to specify the tunnel locations to be investigated. The coloured *Footer* below the pins displays a compressed geology map along the tunnel. The *properties tabs* on the right panel displays the detailed information of the visualised data.

In the following sections, details of each visualisation component (Figure 4) and their data sources (e.g. feature detection process) are explained.

[10]Feature chainage = Ring chainage + distance from TBM cutter head to the feature.

[11]These segments can be multiple rings.

Figure 5: User interface: the bottom pins are associated with TBM locations/chainage.

4.1. Tunnel Geology view

In order to help users to interpret the imaging data, identify (or reduce the ambiguities of) the nature of probable events, a broad view of the geology context along the tunnel route is shown on the user interface in the form of geology maps, which are created by geo-experts in advance based on the surveyed data from boreholes. As shown in figure 6, the *Tunnel geology view* can be accessed using the navigation button on the top of the interface. The *visualisation window* provides a top view and a side view of the whole geology map. Different colour codes represent different ground types and properties. Users can *pan* or *zoom* the maps to see more details. In addition to the main *Tunnel geology view*, a simplified geology map (vertically squashed) is also provided at the bottom of the user interface. It is aligned with the tunnel chainage so that users can easily see the rough geology context at a selected ring when interpret a sensor image. The text summary of the geology information at each ring can also be easily accessed using the *Geology tab* on the right hand side of the panel.

4.2. TBM Parameters View

The TBM parameters view was developed in collaboration with a group of experienced tunnelling engineers within the EU-funded Nettun project, who suggested that the real-time TBM parameters could be visually inspected and used to help evaluate the ground conditions. In addition to manual inspection, automatic analysis of the TBM parameters could also be investigated in the future, e.g. [6]. Implementation of the TBM parameter visualisation view (Figure 7) has been made flexible and allows the visualisation of whatever parameters provided by the ground imaging system (stored in the *TBM Parameters* table). It can be accessed using the parameter button on the top navigation bar. Currently, the ground pressure, cutter head torque, cutter head rotation speed, and thrust force are included. The parameters are visualised as a set of line charts, each of which represents an individual parameter from multiple rings in a tunnel. Users can *pan* and *zoom* the parameter view to see more details. If users want to highlight the parameters at a particular tunnel ring, they can either press the *ctrl+G* key on the keyboard to open a popup window and enter a ring number, or click the corresponding pin on the bottom. A tooltip will appear on the line charts next to the selected ring and display the parameter values.

4.3. GPR and Seismic Data Processing and Visualisation

In this section, both GPR and seismic imaging data is analysed and visualised for interpretation[12]. Integration of the electromagnetic (GPR) and seismic methods (shear-wave) can help detect adverse events based on both dielectric and elastic properties of the targets. Visualisation of the imaging data is implemented in two levels: the first level is to visualise the captured imaging data in an easy-to-understand manner and in a unified coordinate frame; the second level is to highlight anomalous image features and probable events by fusion of multiple sets of imaging data. Since both GPR and seismic sensors are reflection based techniques, in order to calculate the distance from a probable event to the TBM cutter head, the velocity of signals travelling in the surrounding medium must be known. In this work, the velocity (or ground permittivity) of GPR signals is estimated based on the rough ground characteristics; the velocity model of seismic sensors comes out of an inverse modelling procedure as detailed in [29].

[12] N.B. all the imaging data demonstrated in this paper is from a geophysical survey conducted with the aforementioned ground imaging system in Eindhoven, Netherlands in 2015. Two plastic tanks were filled with water and buried in the ground to simulate a water inflow scenario. Materials were gradually filled in to vertically built up the ground, and seven groups of sensor data were captured every $1m$ on top of the target (to simulate in reverse order the TBM drilling process where sensor measurements are concurrent with the ring construction operations).

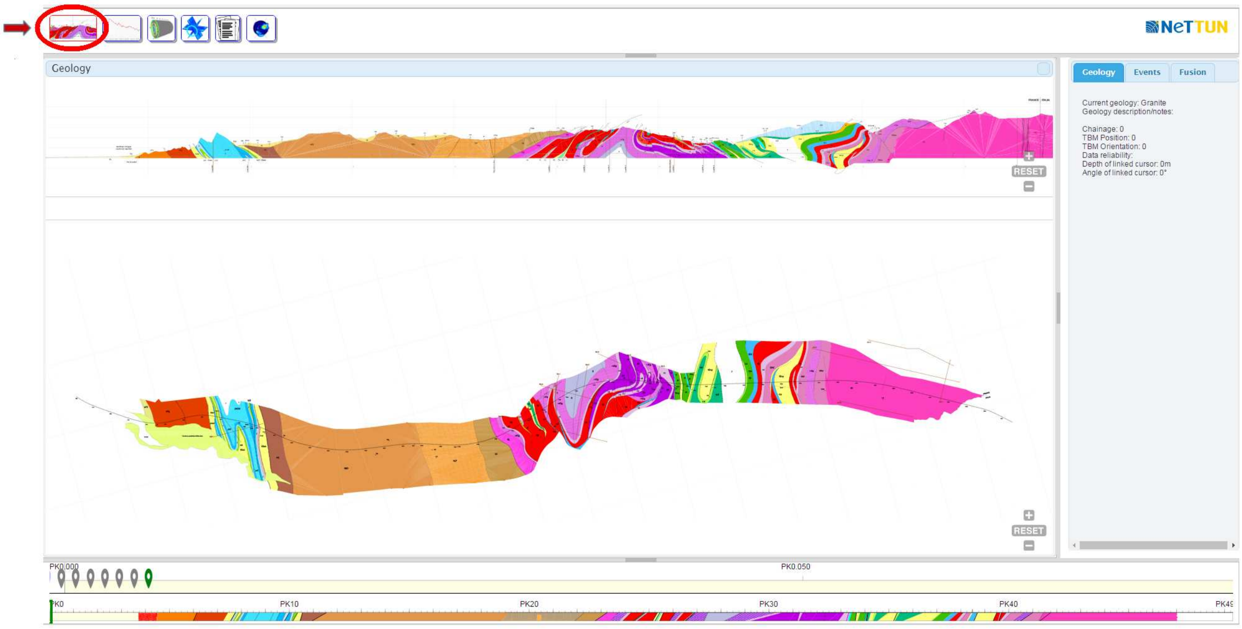

Figure 6: Tunnel geology view.

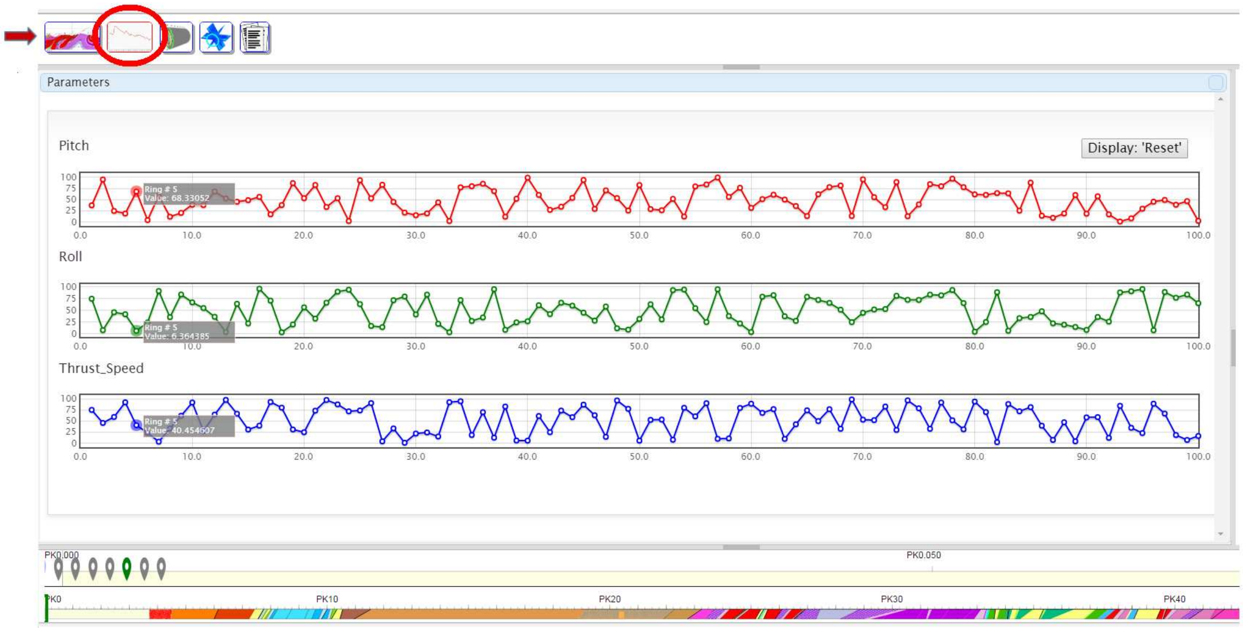

Figure 7: TBM parameters view (when a specific ring is selected, a tooltip appears next to the corresponding data in the visualisation window.)

4.3.1. *Visualisation of the Ground Penetrating Radar Data*

Data acquisition process of the GPR data has been explained in section 3.1. As mentioned above, the designed sensors on a TBM will be configured/rotated in concentric rings (i.e. sensors are placed at three radii sequentially) and each GPR sensor can provide one GPR image at each radii (Figure 8). In our test, there are three such radii and three sets of GPR antennae in the considered scenarios (a low frequency GPR (*LF*) and two high frequency GPR (*HF1, HF2*)), 3×3 GPR images can be captured at each location. In order to make best use of the imaging data captured by different sensors at different locations, a suite of 2D/3D visualisation options were designed and implemented. The *GPR view* (Figure 8) can be accessed using the GPR button from the top navigation bar. The data for a specific tunnel ring can be viewed by selecting the individual pins from the footer.

Cylindrical view and **Planar view.** The on-board GPR antennae rotate around the centre and transmit waves into the ground ahead. Each trace is recorded at a discrete position along an antenna transect, and the combination of these traces provides a 2D vertical slice image through the ground. This image is warped as a cylinder in metre-metric and shown on the user interface with the depth of each image displayed (Fig-

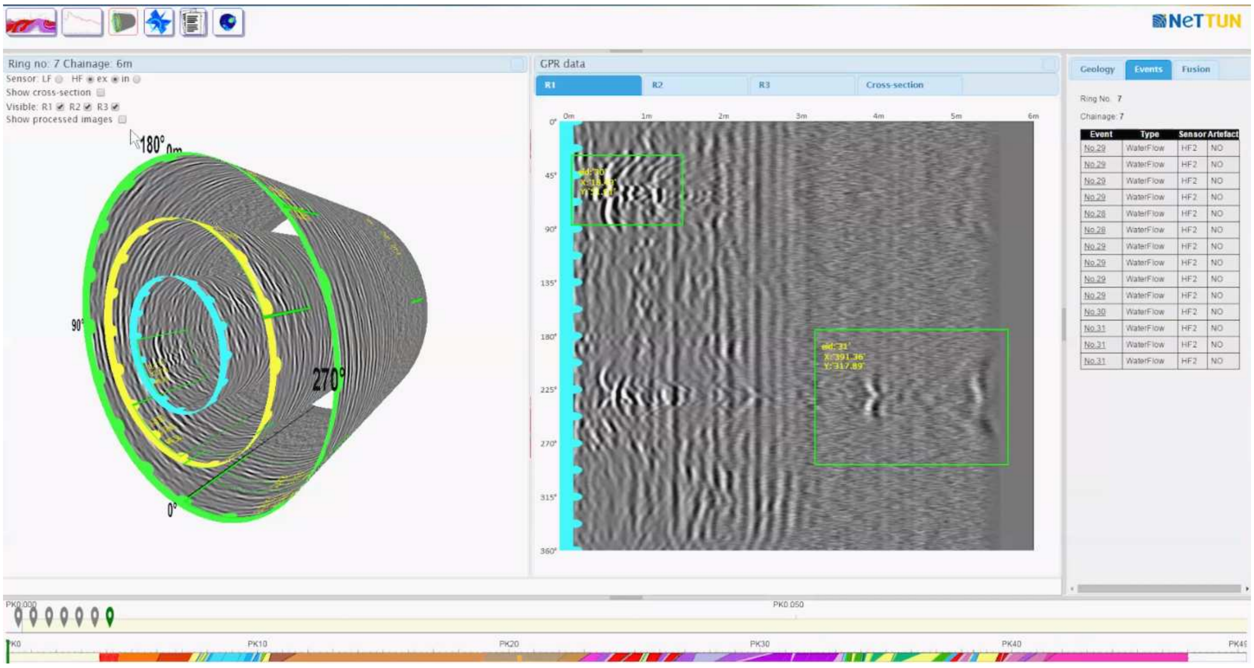

Figure 8: GPR cylindrical view and planar view [34].

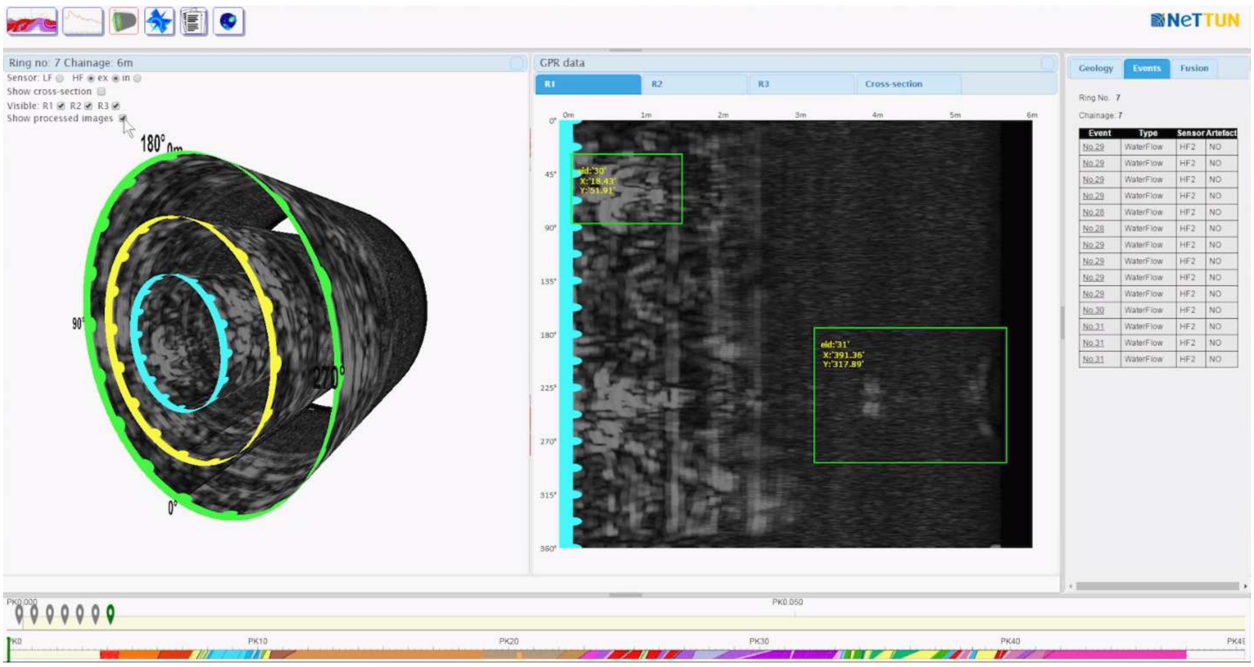

Figure 9: GPR post-processing view.

ure 8 (left)). Users can also rotate and zoom the view using the mouse. The original 2D GPR image is also displayed next to the wrapped image (Figure 8 (right))[13].

GPR post-processing view. User can switch between raw image and post-processed data (Figure 9), which is designed to quickly highlight the anomalous regions with strong amplitude using a simple and fast filter. To do this, the average intensity of the raw image is subtracted from the image; then, the absolute intensity value at each pixel is computed to avoid negative intensity values; after that, an image smoothing filter is applied to obtain the post-processed image.

Switching between different GPR data. As there are GPR data of various frequencies and captured at different radii, users can choose which data to be displayed on the cylindrical view (Figure 10) by switching on the related radio of a a GPR fre-

[13] Note: the green bounding boxes overlapped on the GPR images were derived from the automated feature detection algorithm presented in section 4.3.3.

Figure 10: GPR visualisation options. Users can switch between different GPR sensors and different data capturing radii.

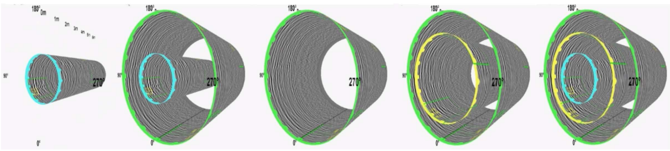

Figure 11: Visualisation of GPR images at different radii.

quency (only one frequency can be selected each time) and ticking the check boxes of the locations of GPR data (multiple radii can be shown at the same time). Users can also switch between different 2D images on the right hand side using the top tabs. Examples of combinations of GPR data at different radii are shown in Figure 11.

GPR interpolated cross-section view. In order to further help visualisation and analysis, an interpolated cross-section view of the cylindrical display is designed (Figure 12(b)). The image on the cross-section view is generated in real-time based on GPR images at different radii (with the same frequency) through the following steps:

a) At first, the GPR image data from different radii is fitted to a structured 3D rectangular grid with vertices shown in Figure 12(a). Local averaging is applied over the angular axis as the data is fitted.
b) Then, a 2D sliced image is extracted from the reconstructed volumetric data perpendicular to the TBM drilling direction at a certain depth *D*. To do this, the 3D rectangular grids are re-sampled to a uniform grid of 2D pixels by linearly interpolating the grey values at each vertex in the mesh. Blue lines in Figure 12(a) are used to illustrate the case of interpolation.
c) Finally, the obtained grey scale image is mapped as a colour map (Figure 12(b), right) which starts at grey level, then goes to orange at a certain threshold to indicate higher values (intensities) on the image. This threshold can be manually controlled by users using the slider bar above the cross-section image (highlighted in the figure with an ellipse).

4.3.2. *Visualisation of the Inverted Seismic Data*

Tunnel seismic sensors measures the reflected signals caused by the acoustic impedance contrast due to ground differences.

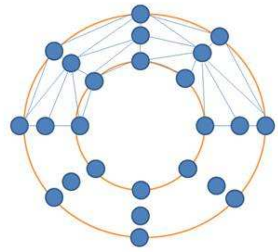

(a) Interpolation of image pixels.

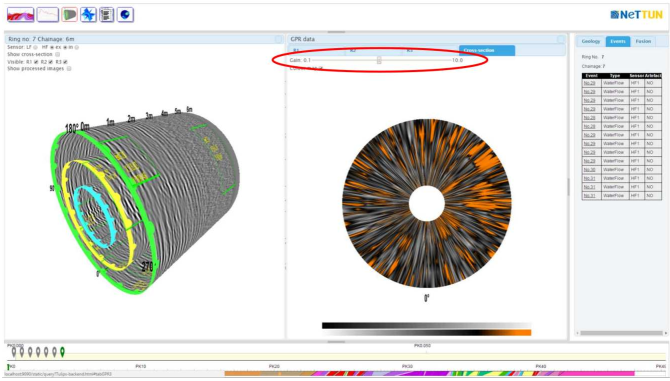

(b) Cross-section view on the user interface.

Figure 12: GPR interpolated cross-section view.

The captured seismic data in our system is first pre-processed and input to a seismic Full-Waveform Inversion (FWI) software [30] to generate a mass-density model and a seismic shear-wave velocity model. In the proposed visualisation platform, both the *Density* and *Velocity* models are visualised (Figure 13) and can be accessed using the Seismic button on the navigation bar or switch between them using the radio buttons.

Similar to GPR data visualisation, both 3D (left window) and 2D (right window) visualisation of the seismic data are provided (Figure 13). In our experiment, three seismic image planes at angles (0, 60 and 120 degrees) were acquired by making use of the rotation of the TBM to these positions; different measurements are combined to obtain data along a particular transect, oriented along one of the diameters of the cutter head [30]. The three acquired image planes are displayed in the left window of the seismic interface (Figure 13). As the visualisation software design is flexible, more image planes can be added if seismic data is captured at more angles. Users can rotate and zoom the view to see more details. In the right window, the 2D seismic images acquired at different angles can be switched using the tabs on the right panel. Seismic data captured at different tunnel rings can also be viewed by clicking on the pins from the footer.

4.3.3. *Detection of Anomalous Features/Events from Multi-sensor Data*

As explained in section 3.3, a *feature* in the imaging data could indicate the presence of an *event* in front of the cutter head. In order to alert TBM operators of potential events

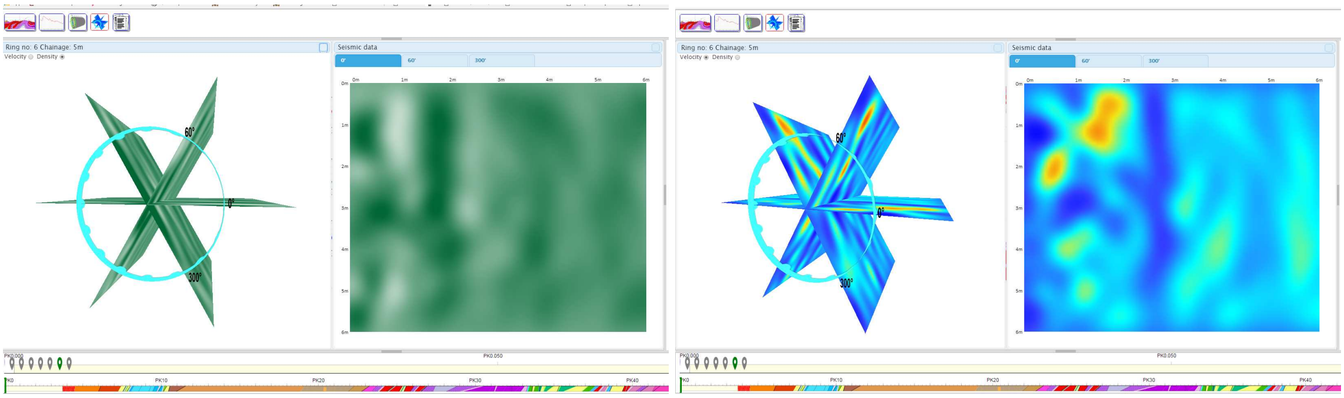

(a) Seismic density model.

(b) Seismic velocity model.

Figure 13: Visualisation of the seismic density and velocity data.

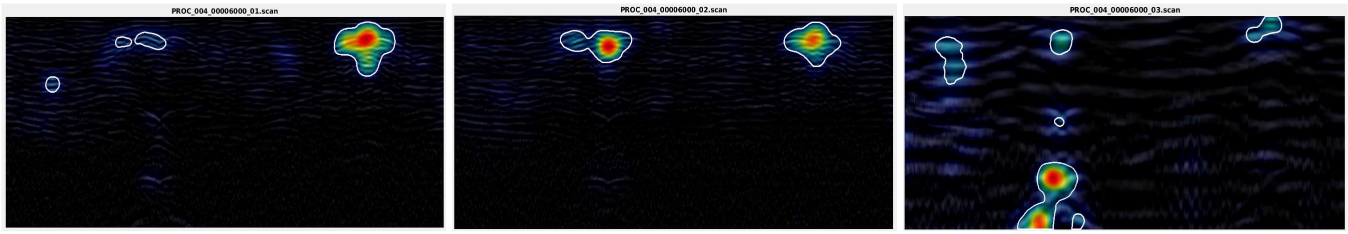

Figure 14: Examples of detected features from GPR images (two high-frequency and one low-frequency images).

and allow the immediate interruption of the excavation before striking them, algorithms (as will be detailed in the following sections) are designed to enable the detection of probable events/obstacles that are of real relevance to the TBM operator. The feature and event detection method used in this work is based on the analysis of image properties and can be executed in near real-time. After collecting sufficient volume of data from real tunnel projects in the future (e.g. with imaging data, geo-experts' annotation and as-built ground truth after excavation), supervised machine learning techniques could be used to build recognition models to further complement the current method.

The image analysis method used in this work is composed of two stages: a) automatic feature qualification in individual GPR and inverted seismic images; and b) fusion/cross-check of GPR and seismic features for event identification.

Feature detection in GPR data. As areas in GPR images with light intensity (except those from ground echo and noise) are generally relating to the underground objects with high dielectric contrast to the surrounding medium, a GPR image can be divided into background and foreground regions using intensity based thresholding methods [35]. In this system, instead of considering each GPR image pixel separately, features are considered as pixels/regions with different intensities with respect to their local neighbouring areas [36, 37]. After applying preprocessing steps (i.e., signal de-wow correction, programmed gain control, horizontal filtering, bandpass filtering and time/depth correction) on a raw GPR image using IDS[14] standard processing software, a 3×3 median filter is applied on the GPR image to remove background noise, followed by subtracting the average of each horizontal trace from all traces to remove ground echo. Then, the GPR image is sub-sampled to s resolutions as I_s, $s \in [S_1, S_2, S_3 \cdots, S_m]$, such as [1/2, 1/4, 1/8], and each sub-sampled image is blurred using a set of Gaussian filters with different standard deviations (σ_1, σ_2). The differences of the Gaussian-blurred images with respect to the original sub-sampled image are summed up and normalised to represent the dissimilarity of pixels with their surroundings in the current image scale. The weighted sum of the difference maps at different image scales is used as the image intensity feature map [34]. This result can be thresholded to find connected areas and the extracted pixels and their associated values are sent forward to the fusion stage explained in the next section. An example of the results from the above mentioned method is shown in Figure 14, in which the extracted connected areas are marked by white contours automatically.

[14] OneVision, IDS, Pisa, Italy. IDS was the commercial partner in the NeTTUN project who designed the GPR antennae.

Features detection in Seismic data. In order to identify potential features in individual seismic image, the $2N$ inverted images (N velocity images and N density images) of the seismic data at a certain chainage are used, where N is the number of angular positions where the acquisition is performed ($N = 3$ in our experiment). An impedance image is first computed using: $I = \rho \cdot V$, where I is the impedance, ρ is the inverted bulk density image and V is the inverted velocity image. Then, the normalised impedance image is thresholded to find the extreme bright/dark regions based on image statistics, which are considered as features in this context.

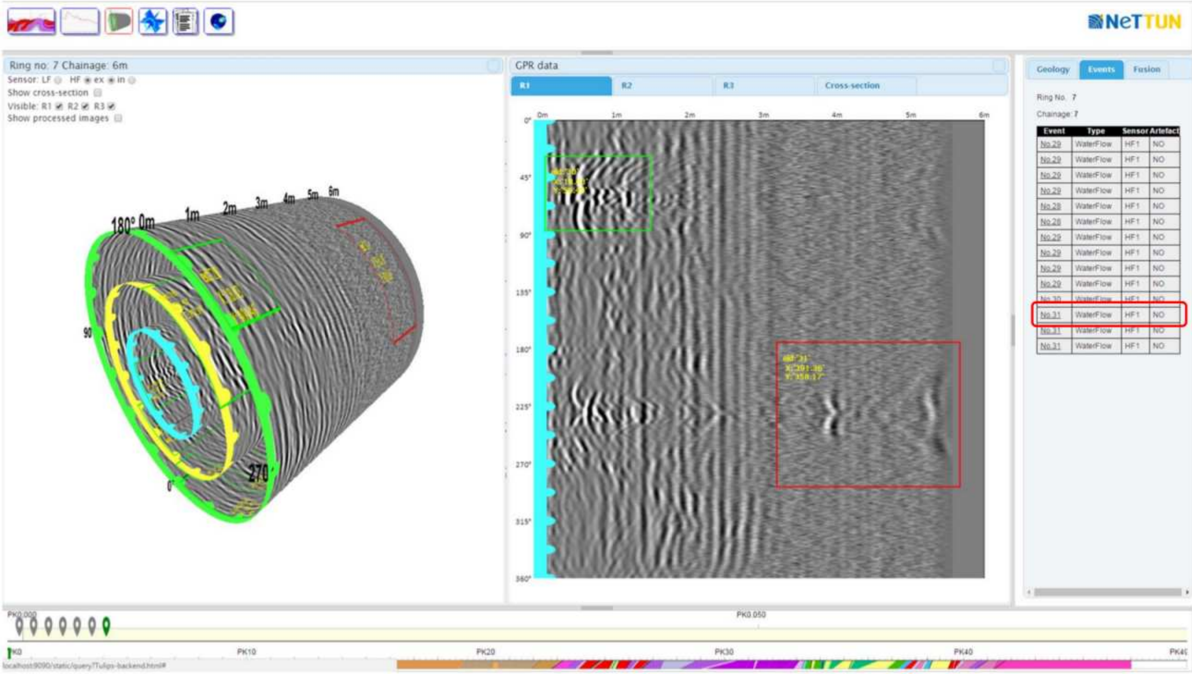

Figure 15: Visualisation of detected features (When the mouse cursor is placed over a feature in the feature table, the corresponding image features on the GPR image are highlighted with red boxes).

Detection and Tracking of Potential Events from Multi-sensor data. The image analysis module sequentially detects features from individual GPR and seismic images. It is possible that the locations of the detected features in individual seismic or GPR images are not consistent (either because the sensors detect a particular object in slightly different locations, or because the feature is not detected at all by one of the sensors). Therefore, the detected features from different sensors and locations are integrated in a 3D accumulator to extract probable events in front of the TBM using a voting strategy: 1) The space ahead of the TBM cutter is divided into a 3D grid. As each 2D pixel on the GPR image plane will contribute a set of weighted "votes" to some 3D spatial locations in the 3D grid, the value of each cell is the accumulation of all of these "votes" dependent on the centre frequency of the radar energy, the depth of targets to the ground surface and the average relative dielectric permittivity of the ground in local area [34]; 2) Image features detected by different sensors are projected into 3D to update this 3D volume. For a detected feature at (x, y) on a 2D GPR image, its corresponding spatial locations can be on a partial sphere surface. For a detected feature on a seismic image, its corresponding location is assumed to be on an image plane. The values of the cells are relating to the partial spheres or image planes and accumulated sequentially; 3) After processing all the GPR and seismic images at one tunnel chainage, the probable events are extracted from the 3D volume based on their values and connectivity. As the ground imaging system moves forward, it may get closer and closer to a potential object ahead, and more information may be gathered by the imaging system. Therefore, 3D events extracted at consecutive tunnel chainages are compared with each other to establish correspondences based on their absolute locations (i.e. 3D centroids and bounding boxes) in the 3D volume (Figure 16).

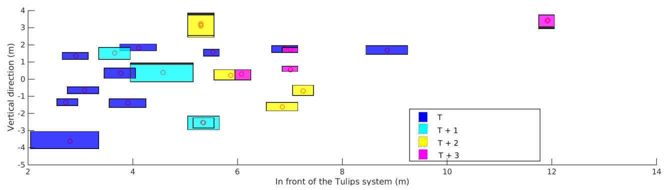

Figure 16: Events tracking: the absolute locations, including the 3D centroids and bounding boxes, of the extracted events are used as the inputs of the tracking method.

Updating Feature and Event Database. After establishing the correspondences between tracked events, the global *Event ID* of previously detected events are propagated and assigned to the corresponding events detected at the subsequent locations. The detected events are then re-projected onto individual sensor image planes (e.g. warped GPR image planes) as validated features. The platform then updates the event and feature database using the information of the extracted 3D events (e.g. global *Event ID*, *3D location* (centroid), *bounding box* (size)) and the corresponding re-projected 2D image features, as well as visualises the detected features and events on the user interface so multiple authorised users can access the platform wherever they are, add annotations, and make final decisions collaboratively.

4.3.4. *Visualisation of the Detected Features and Events*

Based on the updated feature and event database, the detected features and events related to the sensor image(s) selected by the user (as presented in previous sections) are visualised on the user interface.

Visualisation of the detected features. The re-projected image features are shown as green bounding boxes (Figure 15) overlaid on sensor images. The *Features and Events* tab in the properties viewer (right panel) also displays the details of the detected features and events at the selected tunnel location. In the displayed feature/event table, a row relates to a feature in an image. Four attributes of features are currently displayed in the property table (Figure 15), including *Event ID*, *Event Type*, *Type of Sensor*, and whether a feature is considered as an artefact or not. It should be noted that different features can relate to one event and share the same *Event ID*. Whenever a mouse cursor is placed over an *Event ID* in the right-hand side table, the bounding box of the corresponding image features on the GPR image are highlighted (turns from green to red) as shown in Figure 15. This functionality was suggested by users so that they can easily identify/inspect the corresponding features on an image.

Visualisation of the probable events - Front view and Side view. Two views were designed to visualise the probable events from different perspectives: 1) the *Front view* shows the detected probable events seen from the front of the TBM at a selected ring number and can be accessed using the *Interpretation button* from the navigation bar (Figure 17(a)). The front view screen (interpretation) is divided into two views, left for GPR and right for seismic data. 2) The side view window is divided into three horizontal views and can be accessed using the last button from the navigation bar. Each view shows (from top to bottom) the events detected from GPR data, seismic data and fusion of the two data sources. Both the predicted events (30 metres ahead of the TBM) and the *as-built* events (10 metres behind the TBM cutter head) are shown on the image (location of the current TBM cutter head is shown using a vertical yellow lines). Details of the predicted and as-built events are given in the next section. As shown in Figure 17(b), different colour codes are used in the data fusion image, i.e. red for GPR and green for seismic; the *Fusion events properties tab* on the right hand side of the window also displays the event table at a selected chainage, including the *Event ID* and *Event location (X, Y)*. An *Event ID* in the table also possesses a mouse over action, i.e. when mouse cursor is over an event number the corresponding bounding box on the side view images will be highlighted (turns from green to red).

4.4. Context Interpretation: Interactive Expert Input

Based on the discussions with potential users, a user interface was designed to allow human operators to update the nature of a predicted event and to add comments. As shown in Figure 18 (left), the event number shown in the property table under the *Events properties tab* is an HTML anchor, which means that users can click on a certain *event ID* in the table and a popup window form will be opened, known as the experts' evaluation form (Figure 18 (middle)). The evaluation form allows a geological expert to update the event type from a scroll list. Two types of events can be updated, namely *predicted event* and *as-built event*. A *predicted event* is an event propagated from the prediction from previous chainage, and an *as-built event* is annotated after the TBM has excavated. Other fields in this form include quality of acquisition and whether an event is an artefact or not. Experts can also add their comments about the detected event using free text. By clicking on the submit button, the form is submitted and an update success/confirmation message will be displayed (Figure 18 (right)). All of these modifications/annotations by users are recorded in the database for possible further analysis in the future.

5. Test and Discussion

Real imaging data from a field test site was used to demonstrate the feasibility of this system. The test site was built in the Netherlands to gather data using both the radar and seismic subsystems and supply this data to test the data processing and visualisation platform [9]. Five scenarios were built below the surface: karst, anthropogenic structures, inclusion, water inflow and fault. Imaging data from the water inflow scenario is demonstrated in this paper (Figure 8 to 18). In the collected experimental dataset, the detection distance of the seismic sensors is about nine metres, and the detection distances of the low frequency and high frequency GPRs are about three metres and two metres respectively. All the components of the proposed platform, including the data ready communication protocol, the back-end database, the module of feature/event detection, and different data visualisation options as well as the experts' input view, worked smoothly and seamlessly as designed. Both the visualisation interfaces and the detection results revealed and confirmed the location of the buried targets. A video demonstrating the visualisation platform can be found at `http://bit.ly/2E2kz9c`[15]. The platform was also evaluated by TBM engineers, geophysical experts and software consultants in the project from industry who provided positive feedback on it. Indeed they were closely involved in the design of the platform. For example, the geological view was added as the tunnelling engineers we consulted suggested that the geological context could facilitate data interpretation for them. Whilst it is true that the system has not been deployed on an actual TBM due to the end of the project, it is TBM-ready, and the main concerns going forward to this goal are not within the scope of this paper, but rather detailed engineering issues.

In terms of other potential usage of the system, the stored predictions and annotations of adverse geological events in different tunnelling projects could be used in multiple ways. First, the platform could be used as a training platform for junior engineers. By investigating the stored data (e.g. TBM parameters, geological maps, experts' annotation before and after excavation and their explanation) of previous projects, junior engineer can gain a better understanding of imaging data interpretation. Secondly, as the geolocation of adverse geological events as well as their associated imaging data and TBM parameters are stored, when a new project comes closer to a past project stored in the database, the stored adverse geological events could be

[15] Accessed: 2019-04-25.

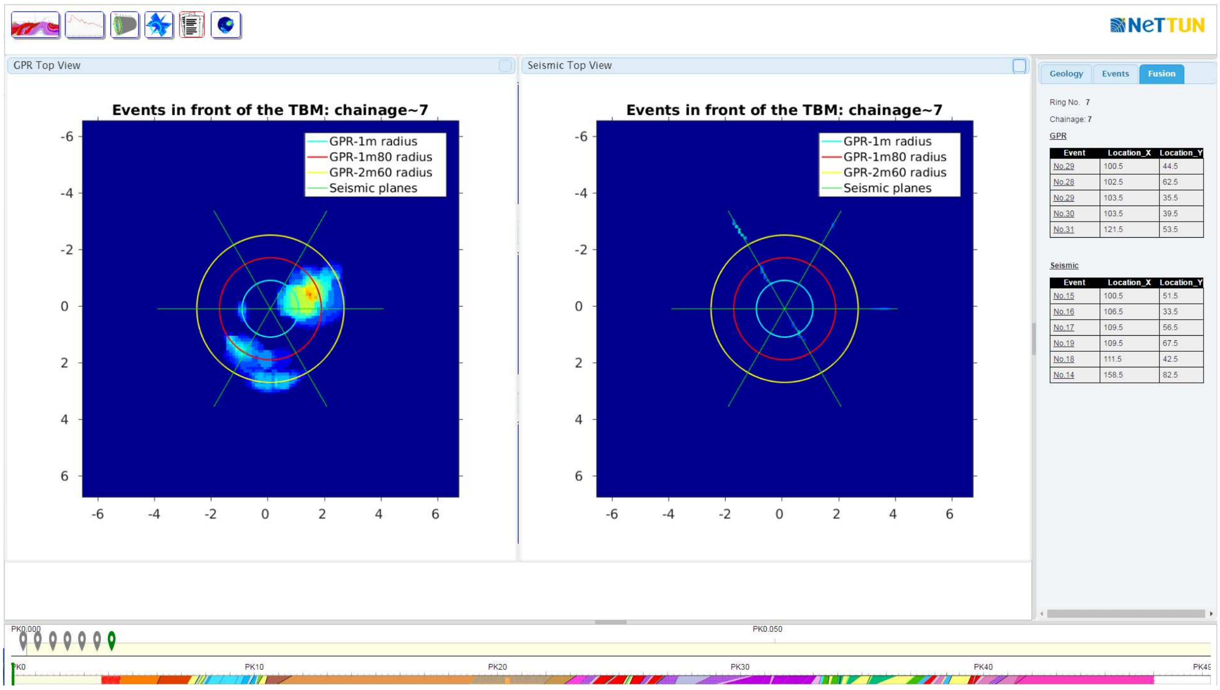

(a) Front view of the probable events.

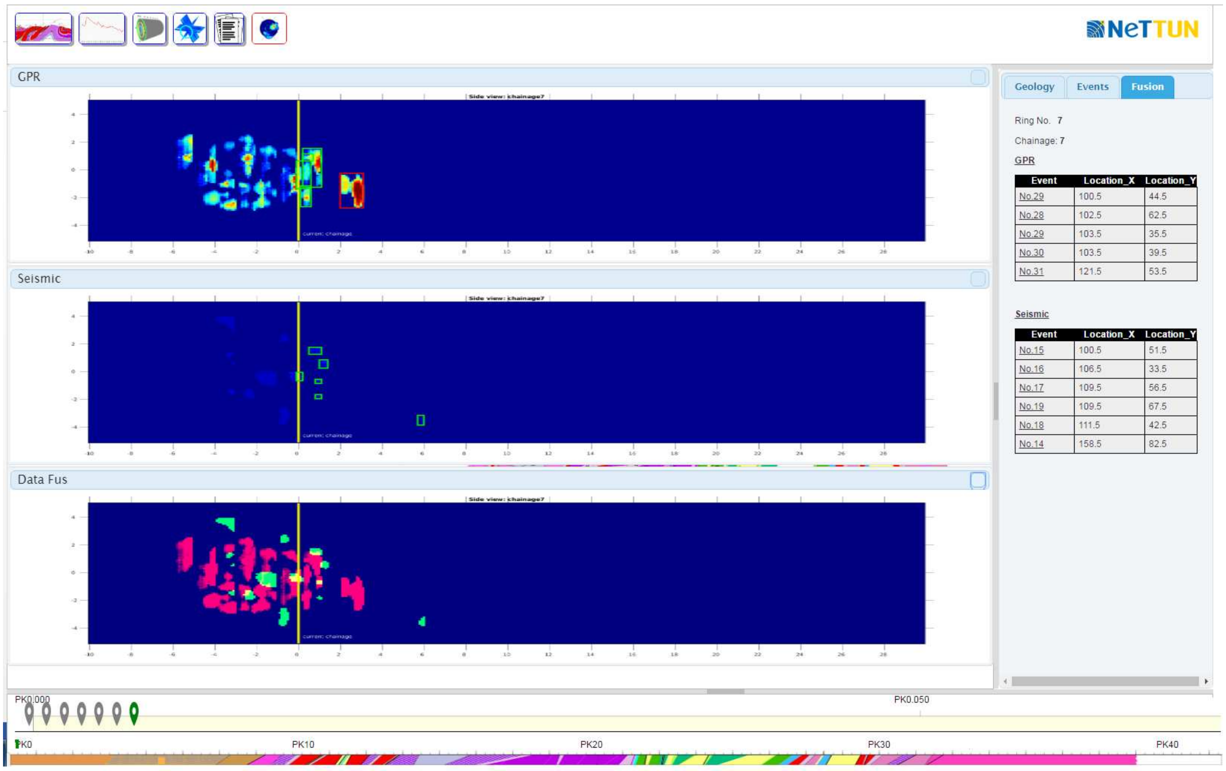

(b) Side view of the probable events.

Figure 17: Data fusion view with detected events: front view and side view.

presented to users (in a 3D-GIS) as the context to help data interpretation, which may also be automated in the future. And thirdly, once we have a large amount of data from different tunnelling projects, including the imaging data, the initially predicted events and the as-built events observed after a tunnel segment has been excavated, these data can be used for machine learning to develop more advanced algorithms for adverse geological events detection and classification.

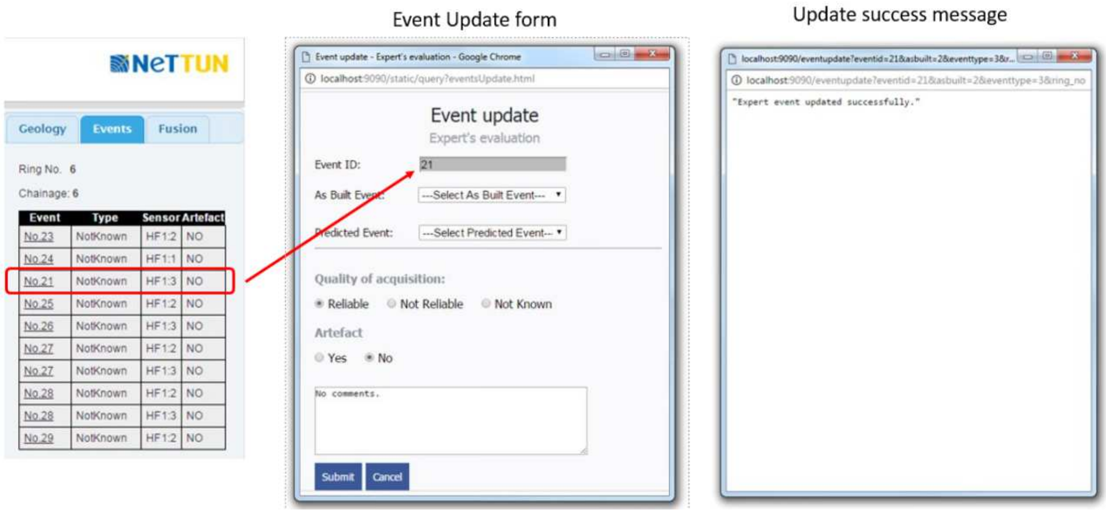

Figure 18: Experts' evaluation forms for updating the attributes of an event.

6. Conclusion

This paper presented a novel web-based visualisation platform for a look-ahead ground imaging system on tunnel boring machines. Linked to a ground imaging system with multiple GPR and seismic sensors, the proposed platform has the functionality of automated imaging data acquisition/storage, 2D/3D visualisation, and automated feature detection by fusion of data from different sensing modalities and different locations. By visualising the ahead-looking imaging data from different perspectives and overlaying the related geological context and TBM parameters, users can gain an understanding of what could be uncovered by subsequent excavations. The web-based design allows geo-experts to remotely (i.e. away from job sites) access and interpret the tunnel imaging data to help identify and alert potential hazards, establishing a collaborative interpretation process. Informative visualisation and user-friendly interfaces were also implemented to maximise the value of data to facilitate the interpretation and decision-making process by TBM operators/geo-experts. The proposed visualisation platform is quite flexible to different sensor models (e.g. sensor frequencies) and configurations (e.g. size/shape of the scanning pattern), so the proposed data processing, management and visualisation framework is also applicable to other ground imaging systems for tunnel inspection or surface geophysical surveys [33], etc.

7. Acknowledgement

We gratefully acknowledge the financial support of the EU under Grant Agreement 280712. We are also grateful to the NeTTUN partners in Technical University of Delft and MI-Partners on accessing and building the Eindhoven test site and developing the seismic system. We thank the project partners in GEO2X and IDS for providing the sensor data used in this paper. We thank the project partners in Incas-partners for providing the suggestions on system design. We also thank the project manager, Thomas Camus, for his tireless efforts in co-ordinating the project.

Appendix A. Database design

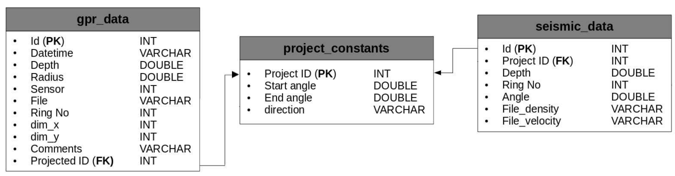

Figure A.19: Relationship diagram of the captured image database.

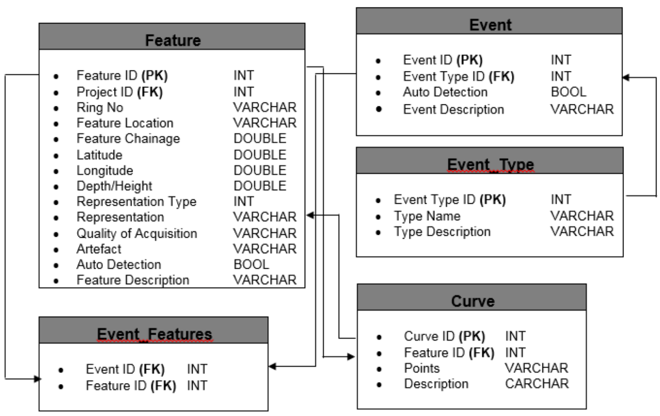

Figure A.20: Relationship diagram of the features and events database.

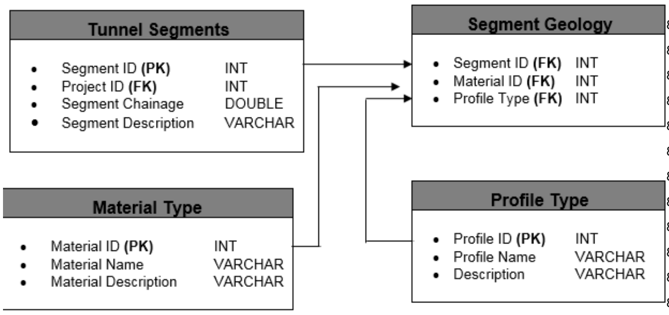

(a) Tunnel geology database.

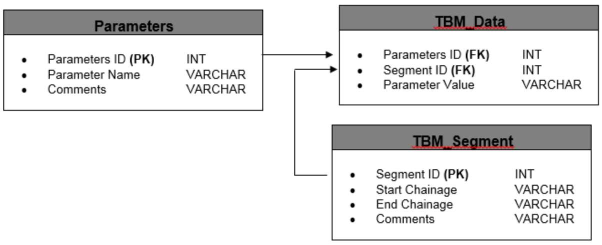

(b) TBM data/parameters database.

Figure A.21: Relationship diagram of the tunnel geology and TBM data parameters database.

[1] S. Li, B. Liu, X. Xu, L. Nie, Z. Liu, J. Song, H. Sun, L. Chen, K. Fan, An overview of ahead geological prospecting in tunneling, Tunnelling and Underground Space Technology 63 (2017) 69 – 94, doi: http://dx.doi.org/10.1016/j.tust.2016.12.011.

[2] X. Huang, Q. Liu, K. Shi, Y. Pan, J. Liu, Application and prospect of hard rock TBM for deep roadway construction in coal mines, Tunnelling and Underground Space Technology 73 (2018) 105 – 126. doi:10.1016/j.tust.2017.12.010.

[3] Y. Zheng, Q. Zhang, J. Zhao, Challenges and opportunities of using tunnel boring machines in mining, Tunnelling and Underground Space Technology 57 (2016) 287 – 299. doi:10.1016/j.tust.2016.01.023.

[4] S.-S. Leu, T. J. W. Adi, Probabilistic prediction of tunnel geology using a hybrid neural-HMM, Engineering Applications of Artificial Intelligence 24 (4) (2011) 658 – 665. doi:10.1016/j.engappai.2011.02.010.

[5] Z. Guan, T. Deng, S. Du, B. Li, Y. Jiang, Markovian geology prediction approach and its application in mountain tunnels, Tunnelling and Underground Space Technology 31 (2012) 61 – 67. doi:10.1016/j.tust.2012.04.007.

[6] T. Yamamoto, S. Shirasagi, S. Yamamoto, Y. Mito, K. Aoki, Evaluation of the geological condition ahead of the tunnel face by geostatistical techniques using TBM driving data, Tunnelling and Underground Space Technology 18 (2) (2003) 213 – 221. doi:10.1016/S0886-7798(03)00030-0.

[7] S. Li, S. Li, Q. Zhang, Y. Xue, B. Liu, M. Su, Z. Wang, S. Wang, Predicting geological hazards during tunnel construction, Journal of Rock Mechanics and Geotechnical Engineering 2 (3) (2010) 232 – 242. doi:10.3724/SP.J.1235.2010.00232.

[8] S. Li, J. Song, J. Zhang, C. Wang, B. Liu, F. Liu, S. Ma, L. Nie, A new comprehensive geological prediction method based on constrained inversion and integrated interpretation for water-bearing tunnel structures, European Journal of Environmental and Civil Engineering 21 (12) (2017) 1441–1465. arXiv:https://doi.org/10.1080/19648189.2016.1170731, doi:10.1080/19648189.2016.1170731.

[9] T. Camus, High performance ground prediction ahead of TBMs - the NeT-TUN system "TULIPS", in: 2016 World Tunnel Congress, San Francisco, California, 2016.

[10] A. Alimoradi, A. Moradzadeh, R. Naderi, M. Z. Salehi, A. Etemadi, Prediction of geological hazardous zones in front of a tunnel face using TSP-203 and artificial neural networks, Tunnelling and Underground Space Technology 23 (6) (2008) 711 – 717. doi:10.1016/j.tust.2008.01.001.

[11] Y. Ashida, Seismic imaging ahead of a tunnel face with three-component geophones, International Journal of Rock Mechanics and Mining Sciences 38 (6) (2001) 823 – 831. doi:10.1016/S1365-1609(01)00047-8.

[12] A. Bellino, L. Garibaldi, A. Godio, An automatic method for data processing of seismic data in tunneling, Journal of Applied Geophysics 98 (2013) 243 – 253. doi:10.1016/j.jappgeo.2013.09.007.

[13] A. K. Benson, Applications of ground penetrating radar in assessing some geological hazards: examples of groundwater contamination, faults, cavities, Journal of Applied Geophysics 33 (1) (1995) 177 – 193. doi:10.1016/0926-9851(95)90040-3.

[14] X. Núñez-Nieto, M. Solla, A. Novo, H. Lorenzo, Three-dimensional ground-penetrating radar methodologies for the characterization and volumetric reconstruction of underground tunneling, Construction and Building Materials 71 (2014) 551 – 560. doi:10.1016/j.conbuildmat.2014.08.083.

[15] H. Cetinkaya, A. Yarovoy, Near field beam patterns of circularly rotating phased array, in: The 8th European Conference on Antennas and Propagation (EuCAP 2014), 2014, pp. 2804–2808. doi:10.1109/EuCAP.2014.6902409.

[16] X. Wang, S. Sun, J. Wang, A. Yarovoy, B. Neducza, G. Manacorda, Real GPR signal processing for target recognition with circular array antennas, in: 2016 URSI International Symposium on Electromagnetic Theory (EMTS), 2016, pp. 818–821. doi:10.1109/URSI-EMTS.2016.7571529.

[17] J. Zou, M. Lu, R. Karumudi, X. Shen, Application potential of ultra-wide band radar for detecting buried obstructions in construction, in: Construction Research Congress 2012 : Construction Challenges in a Flat World, West Lafayette, Indiana, USA, 2012, pp. 1–10. doi:10.1061/9780784412329.088.

[18] J. Park, K.-H. Lee, J. Park, H. Choi, I.-M. Lee, Predicting anomalous zone ahead of tunnel face utilizing electrical resistivity: I. algorithm and measuring system development, Tunnelling and Underground Space Technology 60 (2016) 141 – 150. doi:10.1016/j.tust.2016.08.007.

[19] F. Galeazzi, M. Callieri, M. Dellepiane, M. Charno, J. Richards, R. Scopigno, Web-based visualization for 3d data in archaeology: The ADS 3D viewer, Journal of Archaeological Science: Reports 9 (2016) 1 – 11. doi:10.1016/j.jasrep.2016.06.045.

[20] M. Varela-Gonzlez, M. Solla, J. Martnez-Snchez, P. Arias, A semi-automatic processing and visualisation tool for ground-penetrating radar pavement thickness data, Automation in Construction 45 (2014) 42 – 49. doi:10.1016/j.autcon.2014.05.004.

[21] S. Talmaki, V. R. Kamat, H. Cai, Geometric modeling of geospatial data for visualization-assisted excavation, Advanced Engineering Informatics 27 (2) (2013) 283 – 298. doi:10.1016/j.aei.2013.01.004.

[22] X. Li, H. Zhu, Development of a web-based information system for shield tunnel construction projects, Tunnelling and Underground Space Technology 37 (2013) 146 – 156. doi:10.1016/j.tust.2013.04.002.

[23] Y. Zhou, H. Luo, Y. Yang, Implementation of augmented reality for segment displacement inspection during tunneling construction, Automation in Construction 82 (2017) 112 – 121. doi:10.1016/j.autcon.2017.02.007.

[24] X. Wu, M. Lu, S. Mao, X. Shen, As-built modeling and visual simulation of tunnels using real-time tbm positioning data, in: 2013 Winter Simulations Conference (WSC), 2013, pp. 3066–3073. doi:10.1109/WSC.2013.6721674.

[25] K. Chmelina, K. Rabensteiner, G. Krusche, A tunnel information system for the management and utilization of geo-engineering data in urban tunnel projects, Geotechnical and Geological Engineering 31 (3) (2013) 845–859. doi:10.1007/s10706-012-9547-9.

[26] L. Ding, C. Zhou, Development of web-based system for safety risk early warning in urban metro construction, Automation in Construction 34 (2013) 45 – 55. doi:10.1016/j.autcon.2012.11.001.

[27] G. Manacorda, A. Simi, S. Reynaud, V. Bertrand, M. Sow, E. Martinod, N. Feix, M. Lalande, D. Tran, H. Cetinkaya, A. Yarovoy, The nettun project: Development of a ground prediction sensor, in: 2015 8th International Workshop on Advanced Ground Penetrating Radar (IWAGPR), 2015, pp. 1–4. doi:10.1109/IWAGPR.2015.7292700.

[28] A. Simi, G. Manacorda, The NeTTUN project: Design of a GPR antenna

for a TBM, in: 2016 International Conference on Ground Penetrating Radar (GPR), 2016, pp. 1–6. doi:10.1109/ICGPR.2016.7572648.

[29] W. M. T. T. P. Bharadwaj, G.G. Drijkoningen, R. Jenneskens, A shear-wave seismic system to look ahead of a tunnel boring machine, in: Proceedings of the 2016 World Tunneling Congress, 2016, pp. 1–10.

[30] P. Bharadwaj, G. Drijkoningen, W. Mulder, J. Thorbecke, B. Neducza, R. Jenneskens, A shear-wave seismic system using full-waveform inversion to look ahead of a tunnel-boring machine, Near Surface Geophysics 15 (3) (2017) 210–224. doi:10.3997/1873-0604.2017014.

[31] X. Wu, M. Lu, X. Shen, Computational approach to as-built tunnel invert survey based on processing real-time tbm tracking data, Journal of Computing in Civil Engineering 30 (1) (2016) 232–241. doi:10.1061/(ASCE)CP.1943-5487.0000435.

[32] S. Mao, X. Shen, M. Lu, Virtual laser target board for alignment control and machine guidance in tunnel-boring operations, Journal of Intelligent & Robotic Systems 79 (3-4) (2015) 385–400. doi:10.1007/s10846-014-0113-y.

[33] G. Manacorda, H. F. Scott, M. Rameil, D. Pinchbeck, M. Farrimond, R. Courseille, The ORFEUS project: a step change in ground penetrating radar technology to locate buried utilities, in: NoDig 2007, Rome, 12-14 Sept, 2007.

[34] L. Wei, D. R. Magee, A. G. Cohn, An anomalous event detection and tracking method for a tunnel look-ahead ground prediction system, Automation in Construction 91 (2018) 216–225. doi:10.1016/j.autcon.2018.03.002.

[35] Q. Dou, L. Wei, D. R. Magee, A. G. Cohn, Real-time hyperbola recognition and fitting in GPR data, IEEE Transactions on Geoscience and Remote Sensing 55 (1) (2017) 51–62. doi:10.1109/TGRS.2016.2592679.

[36] L. Itti, C. Koch, E. Niebur, A model of saliency-based visual attention for rapid scene analysis, IEEE Transactions on Pattern Analysis and Machine Intelligence 20 (11) (1998) 1254–1259. doi:10.1109/34.730558.

[37] A. Goldman, I. Cohen, Anomaly detection based on an iterative local statistics approach, in: 2004 23rd IEEE Convention of Electrical and Electronics Engineers in Israel, 2004, pp. 440–443. doi:10.1109/EEEI.2004.1361186.